Journal of Statistical Physics, Vol. 70, Nos. 1/2, 1993

Proton Dynamics in Hydrogen-Bonded Systems

Eric Nylund,[1] Katja Lindenberg,[1] and George Tsironis[2]

We discuss a simplified version of an ice lattice which consists of an alternating sequence of heavy and light masses. The light masses (protons) are each subject to a bistable potential caused by the heavy masses (oxygens). The protons interact with one another, as do the heavy ions. The interactions between the protons and the oxygens modulate the bistable proton potential. This system is known to exhibit kink and antikink solutions associated with mobile ionic defects accompanied by a lattice distortion. We show that at finite temperatures and in the presence of a constant external field on the protons, the defect velocity is a nonmonotonic function of the temperature, reflecting an interesting interplay of thermal effects (noise) and the constant deterministic external forcing in this nonlinear system. We discuss extensions of the model to higher dimensions, and present preliminary results for the proton motion in such networks.

KEY WORDS: Hydrogen-bonded networks; proton dynamics; multidimensional effects; collective motion.

1. INTRODUCTION

The focal theme of this workshop is the response of nonlinear (mainly bistable) systems to simultaneous forcing by noise and by a deterministic periodic signal. The nonlinear nature of a bistable system causes an interplay of these two forces that under certain circumstances leads to "stochastic resonance," an enhanced response of the system to the deterministic signal when the noise parameter values lie in certain specified ranges.[3]

One might broaden this description and view the problem of interest in this workshop as the interplay of deterministic and stochastic forcing of

[1] Department of Chemistry, 0340, and Institute for Nonlinear Science, 0402, University of California-San Diego, La Jolla, California 92093.

[2] Computational Physics Laboratory, Department of Physics, P.O. Box 5368, University of North Texas, Denton, Texas 76203.

[3] The phenomenon of stochastic resonance is described in a number of papers in this issue. Dykman *et al.*[1] describe this effect in a number of systems.

0022-4715/93/0100-0163$07.00/0

nonlinear systems, and the way in which this interplay leads to a variety of types of system responses that are not simple superpositions of the responses of the system to either form of forcing alone. We have been interested in a problem that fits into this broader description.

Our problem arises in the context of models of proton transport in hydrogen-bonded chains and surfaces—for our presentation here the context is perhaps incidental. We will mainly deal with the model itself as one that leads to interesting interplay effects, and avoid arguments as to its applicability to specific physical systems. Nevertheless, we use the terminology associated with real systems, primarily ice, since the models and the parameter values used in numerical simulations are drawn from these associations.

In Section 2 we introduce a streamlined one-dimensional model of a hydrogen-bonded chain and briefly review the possible coherent proton dynamics in such a model. In Section 3 we introduce a finite temperature and a deterministic constant external force, and we discuss the way in which the protons respond to their presence. In Section 4 we preview some of our efforts to extend these studies to two-dimensional systems.

2. ONE-DIMENSIONAL MODELS

A simplified version of an ice lattice is shown in Fig. 1a, and an even simpler one-dimensional version of the model is shown in Fig. 1b. The model consists of an alternating sequence of light ("proton") and heavy ("ion") masses. When the heavy ions are fixed in their equilibrium positions as shown, the potential energy minima for the protons are not located equidistantly from the neighboring heavy ions. Rather, a proton will tend

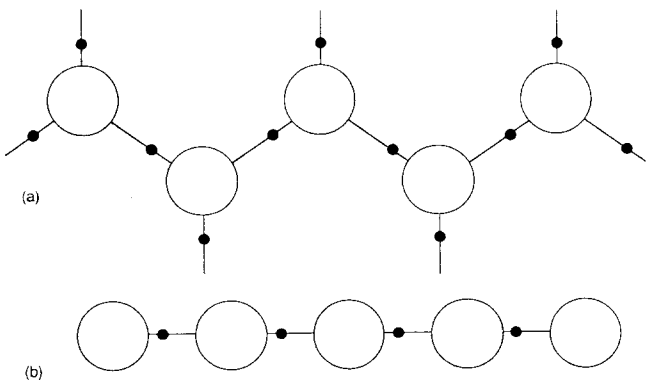

Fig. 1. (a) A simplified version of the cubic hexagonal lattice structure of ice. The large circles represent oxygen atoms, and the smaller black circles represent the protons. (b) A one-dimensional version of the ice lattice.

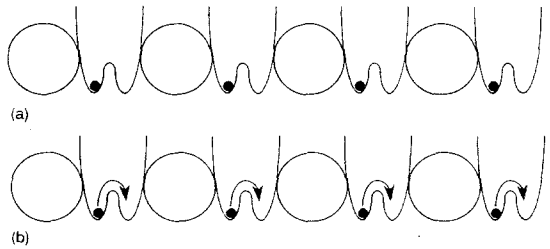

Fig. 2. (a) The symmetric bistable potential of the simplified one-dimensional ice lattice. (b) Translation of each proton from one potential minimum to another represented as a coherent motion.

to lie closer to one of the heavy ions, forming a covalent bond with it, and a hydrogen bond with its more distant neighboring ion. In the figure we have chosen a particular such configuration in which each proton is covalently bonded with the heavy ion on the left. Since in the isolated ion–proton–ion unit there is an equal probability that the proton will bond covalently with either of its neighboring heavy ions, the potential energy surface of each proton is symmetric and bistable, as shown in Fig. 2a. In this figure we have explicitly chosen the same particular proton configuration as in Fig. 1b.

Dynamics that allows a proton to move from one minimum of its bistable potential to the other (as indicated schematically in Fig. 2b) may arise in this model via, for example, a proton–proton interaction. The bistable potential together with this interaction lead very naturally to coherent proton motion. This motion in turn can be associated with the concepts of topological solitons.[2,3] In the simplest versions of the model the heavy ions are fixed, and the proton masses are harmonically bound to one another. The Hamiltonian that determines the dynamics of the chain then is[2,3]

$$H_p = \sum_j \left(\frac{m}{2} \dot{u}_j^2 + \frac{1}{2} m\omega^2 (u_{j+1} - u_j)^2 + V(u_j) \right) \tag{1}$$

where u_j is the displacement of the jth proton from the position midway between the ionic positions, m is the mass of the proton, ω is the frequency that defines the harmonic vibrations of the proton chain, $\dot{u} \equiv du/dt$, and $V(u_j)$ is the average double-well potential on each proton due to the presence of the neighboring ions. A form that has frequently been considered in the literature is

$$V(u_j) = \varepsilon(1 - u_j^2/b^2)^2 \tag{2}$$

Here ε is the barrier height and b is the distance from either minimum of the potential to the maximum at $u_j = 0$. The equations of motion associated

with H_p are obtained by the usual rules of Hamiltonian mechanics. In the continuum limit (i.e., with appropriate limiting procedures whereby the discrete site label n is replaced by a continuous position coordinate x) the equations of motion are of the so-called "ϕ^4"-form and yield "kink" and "antikink" soliton solutions. A kink soliton is formed when two protons surrounding a pair of neighboring ions (called "oxygens" below) find themselves nearer to the more distant minimum of their corresponding potentials with respect to the nearest ion. The instantaneous proton configuration associated with a kink is shown in Fig. 3a, and the corresponding proton displacements from the point midway between the two neighboring heavy ions is indicated in Fig. 3b. In this configuration there is a deficit of positive charge around the oxygen in question. The kink solution has thus been associated with an OH^- "ionic defect." An antikink soliton involves two protons that simultaneously find themselves in the minima nearer to a pair of adjacent oxygens, leading to an excess of positive charge around the oxygen (Figs. 4a and 4b). This solution has been associated with an H_3O^+ "ionic defect."[2,3] Both of these solitons are mobile: for instance, a region which initially has protons all located to the left of center of the individual bonds will have them all located to the right of center once an antikink soliton has moved across the region from left to right. This mechanism can thus describe the concerted motion of all the protons in the chain from one configuration to the other.

The model of proton dynamics as formulated so far does not allow a proton current or proton relaxation. This restriction arises because the protons remain within their original unit cells—the model provides no mechanism for a proton to move from one unit cell to another, but only to shift positions within one cell (i.e., the intercell potential barrier is infinitely high). An important generalization relaxes this constraint imposed by the site potential (2) by introducing instead a doubly periodic

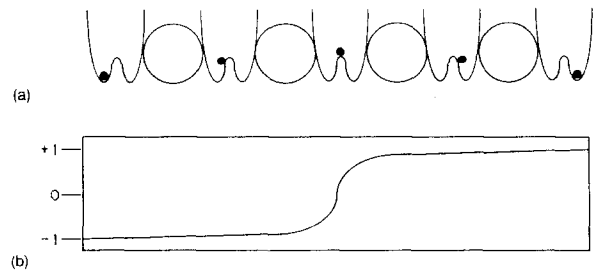

Fig. 3. (a) Proton configuration representing a charge deficit about two central ions. (b) Graphic representation of proton positions within the potential well realized over several lattice sites. This "kink" is associated with an OH^- ionic defect.

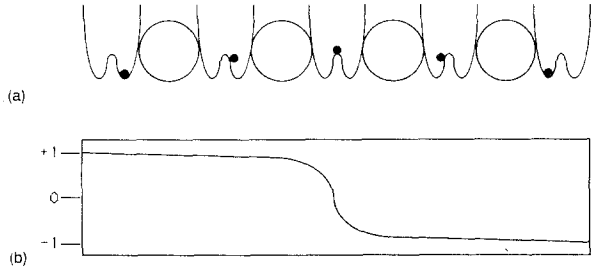

Fig. 4. (a) Proton configuration representing a charge excess about two central ions. (b) Graphic representation of proton positions within the potential well realized over several lattice sites. This "antikink" is associated with an H_3O^+ ionic defect.

potential that allows motion between unit cells.[4,5] A potential that has been used to accomplish this motion is

$$V(u_j) = \frac{2}{1-\alpha^2}\left(\cos\left(\frac{2\pi u_j}{a}\right) - \alpha\right)^2 \tag{3}$$

where a is the lattice constant and $0 < \alpha < 1$. The two-component kink (or antikink) solutions obtained with this model represent "ionic defects" (see above) and "Bjerrum defects" (bond rotations) typically thought to be present in inorganic hydrogen-bonded materials. As before, the ionic defects represent motion within one potential well between two heavy ions; the Bjerrum defects, on the other hand, represent bond motions that allow a proton to actually move along the chain as the covalent bond connecting a proton to a heavy ion rotates from one orientation to another (this motion is most easily visualized in the context of Fig. 1a).

To capture further features essential to the modeling of realistic systems, one must also allow the motion of the heavy ions. Typically in the streamlined models the heavy ion masses are also assumed to be harmonically bound to one another and are subjected to a potential determined by the structure in which the chain is embedded. Furthermore, the motion of the heavy ions modulates the bistable proton potential. The Hamiltonian that determines the dynamics of the chain then consists of several parts[2-6]:

$$H = H_p + H_i + H_{ip} \tag{4}$$

H_p is the proton Hamiltonian (1). The dynamics of the heavy ions are described by the Hamiltonian

$$H_i = \sum_j \left(\frac{M}{2}\dot{U}_j^2 + \frac{1}{2}M\Omega^2(U_{j+1} - U_j)^2 + \frac{1}{2}M\Omega_0^2 U_j^2\right) \tag{5}$$

where M is the mass of the heavy ion, Ω is the frequency defining the vibrations of the chain of heavy ions, and the background potential (here assumed to be harmonic) is characterized by the pseudo-optical frequency Ω_0. Protons and ions are further assumed to interact through

$$H_{ip} = \sum_j \frac{1}{2} \chi U_j (u_j^2 - b^2) \tag{6}$$

where χ is the interaction strength parameter. This interaction is chosen to represent the fact that the double-well potential of the protons is dynamically modulated by the motion of the ions about their average position. Thus, for large ion displacements the effective barrier height is substantially reduced, thereby permitting ion-assisted proton motion (the barrier can even disappear altogether).

The equations of motion for the protons and ions are obtained using the usual rules of Hamiltonian mechanics:

$$\frac{d^2 u_j}{dt^2} = \omega^2 (u_{j+1} + u_{j-1} - 2u_j) + \frac{4\varepsilon}{mb^2} u_j \left(1 - \frac{u_j^2}{b^2}\right) - \frac{\chi}{m} U_j u_j \tag{7}$$

$$\frac{d^2 U_j}{dt^2} = \Omega^2 (U_{j+1} + U_{j-1} - 2U_j) - \Omega_0^2 U_j - \frac{\chi}{M} (u_j^2 - b^2) \tag{8}$$

Analytic soliton solutions for these coupled nonlinear equations have been obtained when $\Omega_0 = 0$ in the continuum limit for a soliton that moves at velocity v_0, the speed of sound for the heavy ion lattice.[2] These solutions describe proton kinks and antikinks accompanied by a deformation of the ion lattice. As a function of the continuous position coordinate x one obtains in this case

$$u(x, t) = \pm b \tanh Rz \tag{9}$$

and

$$U(x, t) = \frac{\chi b^2}{\Omega^2 M} \operatorname{sech}^2 Rz \tag{10}$$

with

$$R = \left[\frac{2}{mb^2 \omega^2} \left(\varepsilon - \frac{\chi^2 b^4}{\Omega^2 M} \right) \frac{1}{1 - v_0^2/c_0^2} \right]^{1/2} \tag{11}$$

where c_0 is the speed of sound of the proton lattice and $z = x - v_0 t$. Equation (9) represents a kink or an antikink, while Eq. (10) is the

accompanying deformation of the ion lattice. The solutions for other velocities (obtained numerically) do not change substantially (note that if the heavy ions are allowed to move, the terminal velocity of the protons is smaller, for otherwise the same parameter values, than is the terminal velocity of the protons if the heavy ions are not allowed to move).[3]

It is interesting (in the context of this workshop) to speculate about possible "internal resonance" effects that might become apparent for certain values of the heavy lattice frequency Ω: it is conceivable that a stochastic resonance effect of sorts arises when this frequency has a particular relation to the characteristic times of the proton dynamics. We have not explored this possibility.

3. FINITE TEMPERATURE AND EXTERNAL FIELD

In order to study the defect motion at finite temperatures, the chain is placed in a heat reservoir. Although not unique,[7] we have chosen to model the coupling between the chain and the reservoir by adding noise and damping terms only to the equations of motion for the heavy ions. The protons are then automatically subject to thermal effects (albeit filtered by the heavy ions) through their coupling to the ions. The equation of motion (8) for the heavy ions is then modified by the inclusion of two new terms:

$$\frac{d^2U_j}{dt^2}+\gamma\frac{dU_j}{dt}=\Omega^2(U_{j+1}+U_{j-1}-2U_j)-\Omega_0^2U_j-\frac{\chi}{M}(u_j^2-b^2)+\frac{f_j(t)}{M} \tag{12}$$

Here γ is a damping coefficient and $f_n(t)$ is a δ-correlated Gaussian stochastic force. The two are related to one another by the fluctuation-dissipation relation (see, e.g., ref. 8)

$$\langle f_j(t)\, f_{j'}(t')\rangle = 2k_{\mathrm{B}}TM\gamma\delta_{j,j'}\delta(t-t') \tag{13}$$

where the brackets indicate an ensemble average over realizations of the force and T denotes the temperature.

The coupled systems of equations (7) and (12) have only been studied numerically. They support narrow "defect" solutions of shapes similar to those obtained in the absence of fluctuating and dissipative contributions. However, whereas those earlier (zero-temperature) defects moved at a finite velocity, the movement of the defects in the presence of fluctuations and dissipation is random: the defect centroid performs a random walk of vanishing average velocity. Net (nonzero-average-velocity) defect motion at finite temperatures can only take place if one applies an external deterministic force to the system. We implement such a force by adding a

suitable contribution to the proton equation of motion (7), which now becomes

$$\frac{d^2u_j}{dt^2} = \omega^2(u_{j+1} + u_{j-1} - 2u_j) + \frac{4\varepsilon}{mb^2} u_j\left(1 - \frac{u_j^2}{b^2}\right) - \frac{\chi}{m} U_j u_j + \frac{eE}{m} \quad (14)$$

The electric field E is constant in our studies, and only its effect on the protons is considered. In the presence of this field, the (numerical) defect solutions have a finite average terminal velocity on which are superimposed velocity fluctuations.[9] These fluctuations, also caused by thermal effects, are not analyzed here.

A typical defect and its accompanying lattice distortions are shown in Fig. 5. Note that approximately 5 or 6 lattice sites participate in a substantial way in the defect and its accompanying lattice (heavy ion) distortion. Also note the fluctuations in the defect velocity that can be clearly discerned in this figure. Figure 6 shows the propagation of a defect at two different temperatures—one can clearly ascertain the variations in the velocity as a function of time at each temperature, as well as the differences in the average velocities at different temperatures: the defect at 190 K clearly moves *more rapidly*, on the average, than does the defect at 210 K.

The behavior shown in Fig. 6 is representative of the fact that the

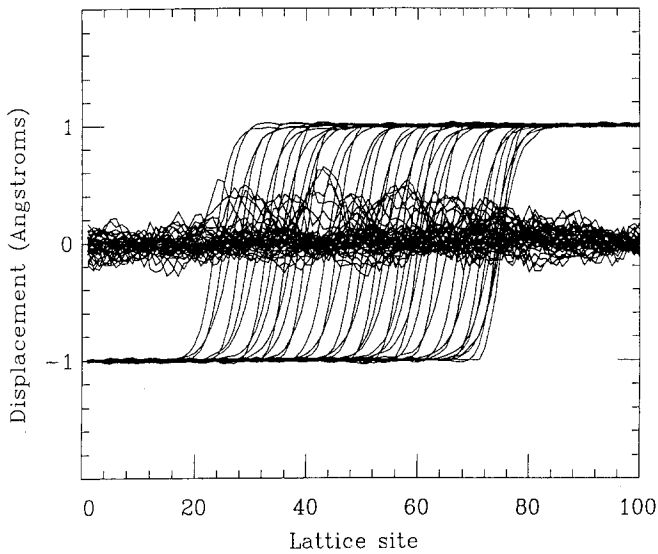

Fig. 5. A kink-type defect and its accompanying lattice distortions. Simulation generated at a temperature of 140 K.

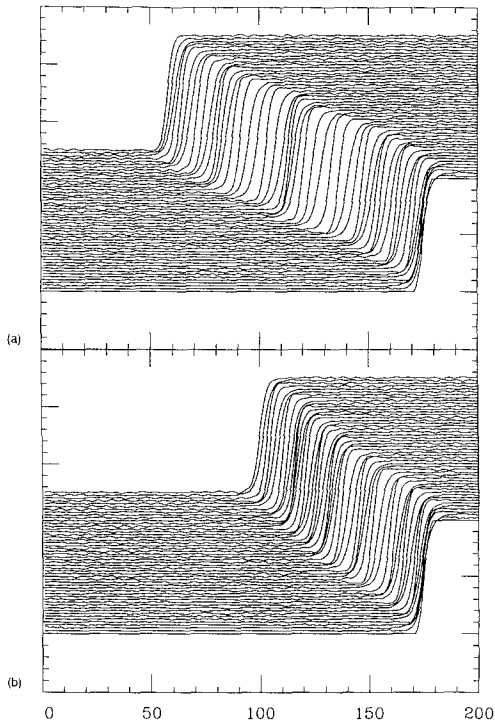

Fig. 6. Trace of a propagating kink-type defect for 250 time units. Displayed on the x axis is the lattice site coordinate, and on the y axis the proton displacement within the potential well (u_j). Time is advancing away from the viewer. (a) Simulation at 190 K. (b) Simulation at 210 K. Both defects are simulated under identical conditions except for the temperature.

average velocity of the defect (which would vanish in the absence of the field) is determined by an interesting *interplay* of field and noise effects. This interplay is more clearly shown in Fig. 7, where we exhibit the average terminal defect velocity as a function of inverse temperature for two different field values. These results were obtained by averaging five numerical simulations of Eqs. (12) and (14) on 100 lattice sites for each temperature of the system at the respective field values. The equations of motion were numerically integrated using a fourth-order Runge-Kutta algorithm. To make these equations appropriately dimensionless, the following units were picked as the standards within the simulation[9]: time unit equal to 1.0214×10^{-14} sec, mass unit equal to 1 amu, and length unit equal to 1×10^{-10} m. The parameter choices were guided by the values appropriate for ice and agree with those chosen in other numerical investigations in this field[3,5,6]: $\varepsilon = 2.0$ eV, $b = 1.0$ Å, $a = 5.0$ Å, $m = 1.0$ amu, $M = 17.0$ amu,

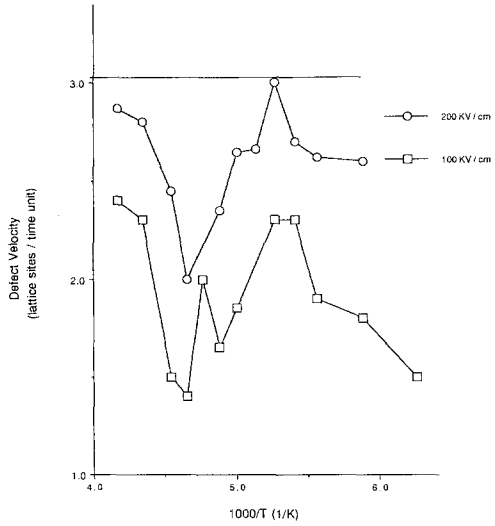

Fig. 7. Average defect velocity as a function of inverse temperature for two field values.

$\omega = 5.87 \times 10^{-14}\ \text{sec}^{-1}$, $\Omega_0 = 1.80 \times 10^{-13}\ \text{sec}^{-1}$, $\Omega = 5.87 \times 10^{-13}\ \text{sec}^{-1}$, $\chi = 0.10\ \text{eV/Å}^3$, and dt is typically taken as 0.05 time units.

As the temperature increases, the defect mobility rises and peaks around 190 K. Subsequently it drops, reaches a minimum at approximately 210 K, and then rises again. This markedly *nonmonotonic* behavior in this temperature regime is a fairly robust effect for different values of the electric field. We have indications (from numerical simulations) that upon extending the temperature range further, other decreases/increases in the defect velocity occur, i.e., that this oscillatory behavior is repeated. We note that results of proton current measurements in ice show similar nonmonotonic behavior,[10,11] although we recognize that the relations between our simple one-dimensional model and the transport mechanisms that might be associated with these current measurements in the far more complicated ice crystals are tenuous.

The temperature dependence of the defect velocity calculated from our model can be directly attributed to the nonlinear nature of the proton potential. To understand this behavior, consider first what happens in the absence of a field. In this case, the proton defect is symmetric around a central proton which lies at the top of the potential barrier (proton 1 in Fig. 8a). Adjacent on either side of the defect center there are pairs of protons that lie lower on the potential energy surface and that have equal potential energies (protons 2 and 3; protons 4 and 5; etc.). Thermal noise causes these protons to execute a random walk, with an equal (temperature-

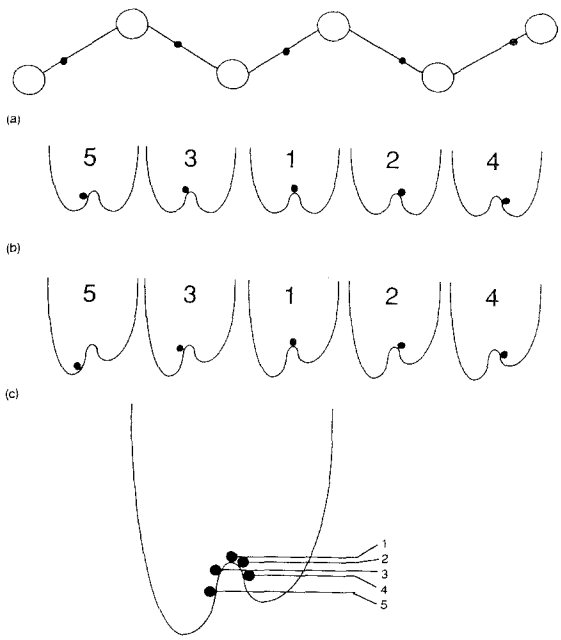

Fig. 8. (a) A defect in a quasi-one-dimensional hydrogen-bonded chain, and the position of the protons in the corresponding symmetric potentials. (b) An external (negative) electric field breaks the symmetry of the potential well. (c) Proton hierarchy of potential energies within the asymmetric bistable double well.

dependent) probability of pulling the protons on either side of the barrier over the barrier—those closest to the top with greatest probability. As one or the other is pulled over the barrier, the center of the defect is buffeted back and forth with equal probability in either direction.

When a field is applied, the symmetry of the potential is broken and the protons that formerly had the same potential energy no longer do (Fig. 8b). Thus, for example, proton 2, which is next to the center of the defect in the direction opposite to the field, is closer to the top of the barrier than is proton 3. The "ranking" of the proton distance from the top of the barrier alternates from one side of the center of the defect to the other (Fig. 8c). At low temperatures, the proton that lies closest to the top of the barrier (proton 2) now has a greater probability of crossing the barrier than does proton 3, and this imbalance of probabilities continues (and in fact increases) with increasing temperatures for some range of temperatures. Each passage of proton 2 over the barrier is accompanied by a push on proton 1 in the direction of the field (and hence an increase in the defect velocity); the passage of proton 3 over the barrier is accompanied by

a pull of proton 1 in the opposite direction (thus tending to decrease the defect velocity). Thus, the net effect is an increase in the average defect velocity.

As the temperature is increased further, there comes a point where proton 3 easily crosses the barrier, thus counteracting the effects of proton 2 and slowing the defect down. Within some temperature range the crossing of proton 3 becomes increasingly easier relative to 2 and the velocity decreases. When the temperature is increased further, proton 4 enters the picture and thus leads to an increase in the defect velocity, until proton 5 enters the picture, when the defect slows down again. Actually, the temperatures shown in the simulation results are too low for protons 4 and 5 to cross the barrier. However, the thermal motions of these protons

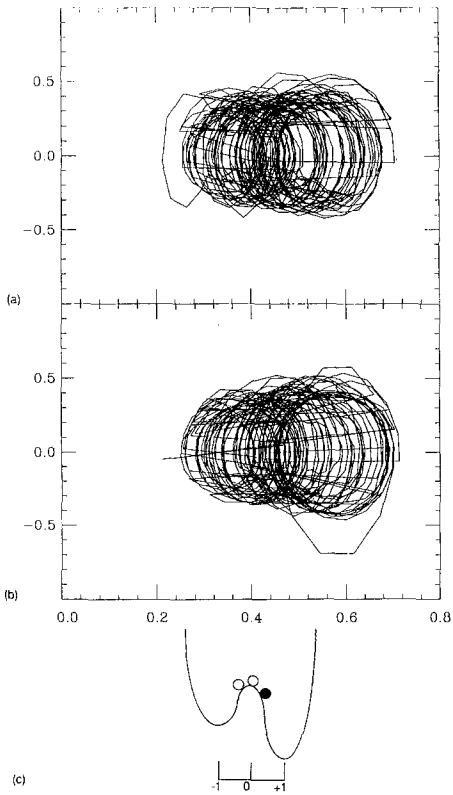

Fig. 9. Phase space plot (momentum vs. position) of proton immediately downfield of the centroid of the defect. (a) Simulation at 185 K; (b) simulation at 215 K. The average velocity of the defect is greater at the lower temperature. (c) Position of a downfield proton (dark circle) in relation to the centroid of the defect.

on "their" side of the barrier have an influence on protons 2 and 3, respectively. Proton 4 has a greater impact on proton 2 than does proton 5 on proton 3 in the temperature ranges studied. Thus, the defect velocity again increases with temperature after reaching a minimum.

A visualization of this effect can be achieved via a phase space plot (momentum vs. position) of proton 3 in the traveling defect, as shown in Fig. 9. The upper plot is for a simulated temperature of 185 K, and the lower for 215 K, for which the average terminal velocities of the defects are respectively faster and slower. The trace of the faster defect shows a slightly greater phase density in the region of positive momentum. This represents the proton traveling toward the minima of the potential well, contributing to the overall motion of the defect in the direction of the applied electric field. Contrast this with the behavior of the slower defect, which has a more uniformly distributed phase density in the positive and negative momentum regions. In addition, there are striking examples of the "crossing" behavior described earlier (plotted as the straight lines which zigzag toward the local maximum of the double-well barrier).

Thus, the *oscillarory* behavior of the defect velocity in the presence of a *constant* electric field and thermal fluctuations is clearly a consequence of the interplay of the two forces in the nonlinear potential.

4. TWO-DIMENSIONAL PROTON DYNAMICS

We are ultimately interested in modeling proton transport in two-dimensional systems, in the context of particular systems of physical interest. One of these is cyclodextrin, in which complex hydrogen-bonded networks may form on the outer and inner surfaces of the cylindrical structures formed upon crystallization.[12] Experimental evidence indicates that the proton dynamics on these networks may be coherent, reminiscent of the soliton like dynamics just described. Cyclodextrin (CD) has dramatic conductivity properties that can perhaps be understood in terms of such a model. For instance, the electrical conductivity of a CD stack varies by three orders of magnitude when the hydration is changed from five water adduct species per CD ring to six water adduct species per ring.[13] Such dramatic changes may result if a "threshold" degree of hydration is necessary for the network to be sufficiently connected to support coherent motion.

We are also interested in understanding the dynamical molecular mechanisms responsible for active proton transport across biological membranes. In this context, we again believe that an extension of the one-dimensional models described earlier may provide useful insights. Several theoretical models as well as experimental results indicate that biological

proton transport systems may consist of low-dimensional chains of alternating hydrogen and covalent bonds.[14–18]

To study actual proton transport mechanisms in one-dimensional geometries it is necessary to allow a proton to leave its local bistable potential, which in turn requires the consideration of, for example, a doubly periodic potential, as previously mentioned. Furthermore, to account for realistic details in the physical systems of interest to us, it is necessary to consider more complex, higher-dimensional models. Several nontrivial issues surround the construction of such models.

First, it is noted that the harmonic forces that are introduced to allow the protons to interact with one another have the unphysical feature of growing in magnitude rather than decreasing with proton separation. Instead, we use an exponentially decreasing interprotonic force to simulate a more realistic screened Coulomb potential. Such a potential recognizes the presence of the heavy ions in the proton–proton interaction.

Second, the actual form of the two-dimensional potential must be chosen with care. It is tempting to generalize the double periodic model to a higher-dimensional surface (e.g., by converting scalar to vector displacements and single to multiple indices; see Fig. 10). However, it turns out that with any such generalization it is impossible to allow the protons

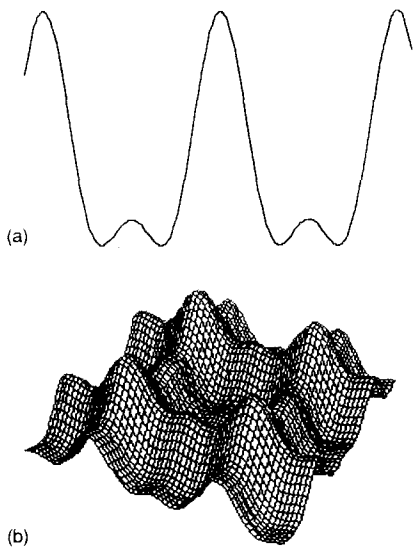

Fig. 10. (a) Doubly periodic potential model as described in Eq. (3). (b) The two-dimensional analog of the double-barrier model generated by converting single to multiple indices and scalar to vectorial displacements.

to move freely while preserving the proper electrical balance at all times—local unphysical net forces arise as an artifact of any such construction.

In order to satisfy the zero-net-force constraints, we have instead opted for a two-dimensional network in which each heavy ion is surrounded by a spherically symmetric potential.[19] The average potential exerted on proton **j** located at position $\mathbf{r}_j$ by heavy ion **k** located at $\mathbf{R}_k$ may be written as

$$V(\mathbf{r}_j - \mathbf{R}_k) = \alpha \exp[-\zeta(\mathbf{r}_j - \mathbf{R}_k)^2] - \beta \exp[-\omega(\mathbf{r}_j - \mathbf{R}_k)^2] \qquad (15)$$

(see Fig. 11). This potential generalizes (3) and shares with it the double-barrier feature, one barrier at the origin and the other at a distance determined by the parameter values in (15). In dynamical simulations of a multipotential network, each proton experiences only the potential due to the nearest heavy ion—if a summation over all heavy ions acting on each proton is performed, unphysical features such as the loss of the local potential barrier along the molecular bond coordinate can occur. The rapid (exponential) decay of the potential justifies our procedure. Furthermore, we note that this model allows the protons to equilibrate spatially to an electrically neutral configuration within the network. It should be noted, however, that in the strictest sense the rotational barrier is no longer present in this extended potential. An intermediate barrier about the origin is present, but protons are highly unlikely to traverse this, as other, less energetic routes are available. Within our model, to "rotate" about the ion–ion bond axis the proton motion typically traverses the potential minima. While it still must pay the energetic cost of overcoming the net repulsive electrostatic forces of the other protons, this is generally much less than the value traditionally assessed to a bond-breaking rotation

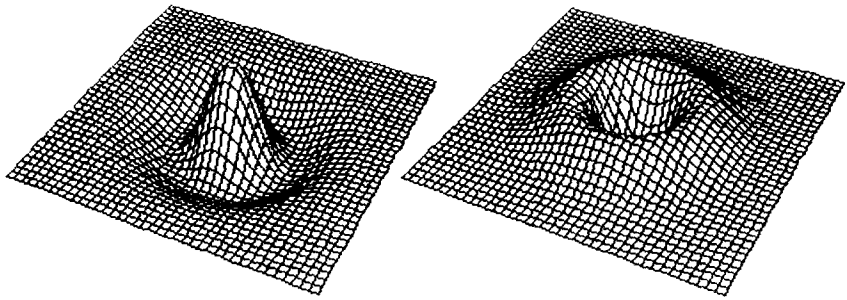

Fig. 11. (a) Exponentially decaying pair-type potential plotted from $+2$ to -2 length units on either axis. $\alpha = 3.15$, $\beta = 4.0$, $\zeta = 1.8$, $\omega = 3.0$. (b) Reversed potential, displayed for detail.

within the crystal lattice. Simulation of this process for multiple sites demonstrates a network of paired protons "flipping" back and forth from one set of equilibrium positions to another, in turn influencing neighboring pairs to mirror this process. Experimentally, recent neutron diffraction studies of hydrogen-bonded networks show similar dynamic behavior.[12]

The Hamiltonian for the protons in a network of fixed potentials of the form (15), with no consideration of the dynamics of the heavy ions, is given by

$$H = \sum_{\mathbf{j}} \frac{m}{2} \dot{\mathbf{r}}_{\mathbf{j}}^2 + \sum_{\mathbf{j},\mathbf{k}}{}' V(\mathbf{r}_{\mathbf{j}} - \mathbf{R}_{\mathbf{k}}) \tag{16}$$

As before, $\mathbf{r}_{\mathbf{j}}$ and $\mathbf{R}_{\mathbf{k}}$ indicate the positions of the protons and heavy ions, respectively. The prime on the second sum stresses the restriction mentioned above whereby each proton is only associated with its nearest ion. Note that the model allows us to study a variety of hydrogen-bonded materials by simply altering the underlying structure that defines the average locations of the heavy ions. The next step in the process is to allow the heavy ions to move as well, a step that we have not yet implemented. Note that the coupling between the motions of the protons and heavy ions is already incorporated in the **R** dependence in Eq. (16).

To simulate the presence of thermal effects, one might proceed as in the one-dimensional case, that is, by adding fluctuating and dissipative forces to the equations of motion of the heavy ions. Since we are at this point not considering the dynamical evolution of the heavy ions and hence do not yet wish to deal with explicit ion equations of motion, we must find an alternative procedure. A procedure that retains the notion that the heavy ions (rather than the protons) are the ones directly connected to the heat bath and that can be implemented independently of any other assumed dynamics for the heavy ions is the direct addition of fluctuations to the positions **R**. We have implemented this procedure (without yet implementing any other heavy ion dynamics) by assuming that the maximum of the potential centered at $\mathbf{R}_{0,\mathbf{k}}$ at zero temperature fluctuates about this value at finite temperature, so that the maximum position acquires a time dependence $\mathbf{R}_{\mathbf{k}}(t)$. The temperature is fixed by requiring that the fluctuations about the average satisfy the relation

$$\langle (\mathbf{R}_{\mathbf{k}}(t) - \mathbf{R}_{0,\mathbf{k}})^2 \rangle = \frac{2k_{\mathrm{B}}Tt}{M\gamma} \tag{17}$$

for each **k**. As before, γ is the damping coefficient. Damping is added phenomenologically to the proton equation of motion to balance these

fluctuations. The equations of motion for the protons may then be written as

$$\frac{d^2\mathbf{r}_j}{dt^2} = -\gamma \frac{d\mathbf{r}_j}{dt} - \frac{dV(\mathbf{r}_j - \mathbf{R}_k(t))}{d\mathbf{r}_j} - \sum_i \kappa \exp[-\xi |(\mathbf{r}_j - \mathbf{r}_i)|] \qquad (18)$$

Here κ and ξ are the parameters that characterize the electrostatic interproton interaction. The kinetic energy is monitored throughout the simulation and is found to have the expected value of $k_B T/2$ per degree of freedom, in accordance with the equipartition theorem.

Recent simulations of this model system are proving encouraging. In Fig. 12 the trace of the proton motions is shown for such a quasi-two-dimensional hydrogen-bonded network. The accompanying diagram illustrates the traveling defect as it works its way through the system. Note

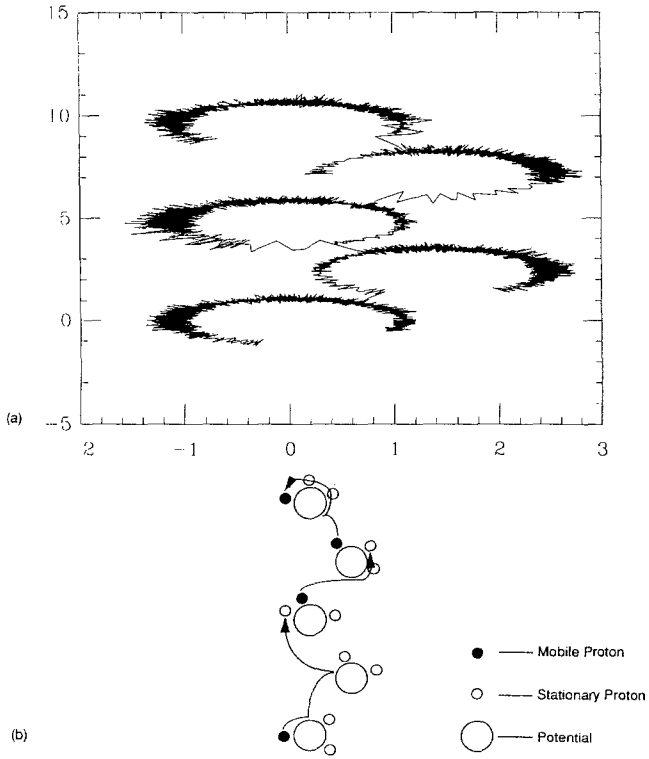

Fig. 12. The trace of proton motions in a pair potential network at a temperature of 330 K, and influenced by a field of 100 kV/cm. Potential parameters are $\alpha = 12.0$, $\beta = 8.5$, $\zeta = 4.5$, and $\omega = 0.05$. (b) A simplified diagram illustrating the motion of the proton traversing the network.

one feature that is immediately obvious: the transferred proton is not necessarily restrained to be the adjacent down-field proton, as it is in the one-dimensional models. In general (although it is highly unlikely) a single proton could wend its way through the entire chain.

Refinements of this model are in progress and will undoubtedly advance our understanding of the dynamics of hydrogen-bonded collective motions. In particular, we are in the process of implementing the summation of pair potentials to yield a potential with notational barriers that are not solely a function of the proton–proton electrostatic interactions, as well as an accurate mapping scheme to realistically project three-dimensional proton networks onto a two-dimensional surface.

5. CONCLUSION

We have discussed a coupled one-dimensional system of particles in bistable potentials that give rise to solitonlike "defect" solutions. In the presence of an external dc field and thermal fluctuations/dissipation, the velocity of the "defect" solutions is a nonmonotonic function of the temperature. This behavior results from the nonlinear nature of the potential and the consequent interplay of the dc field and the thermal effects.

It is our hope that generalizations of these models to two dimensions may contribute to the understanding of proton transport in a variety of systems, perhaps including proton transport across biological membranes. Several questions germane to this particular field that may be answered by our studies include the role of dimensionality in the propagation of nonlinear defects, the ability of charged defects to traverse channels against large fields, and the ability to thermally generate spontaneous defects in inorganic and biological materials.

ACKNOWLEDGMENTS

Two of us (K.L. and E.N.) gratefully acknowledge the partial support of this research by the National Science Foundation through Grant No. DMR-86-19650-A1 and by the Donors of the Petroleum Research Fund, administered by the American Chemical Society. One of us (G.T.) acknowledges partial support by the University of North Texas. The work of Stephanos Pnevmatikos was instrumental in inspiring us to continue along the road that he so brilliantly opened. We miss him.

REFERENCES

1. M. I. Dykman, D. G. Luchinsky, R. Mannella, P. V. E. McClintock, N. D. Stein, and N. G. Stocks, *J. Stat. Phys.* **70**:463 (1992).

2. V. Ya. Antonchenko, A. S. Davydov, and A. V. Zolotaryuk, *Phys. Stat. Sol.* (*b*) **115**:631 (1983).
3. M. Peyrard, St. Pnevmatikos, and N. Flytzanis, *Phys. Rev. A* **36**:903 (1987).
4. St. Pnevmatikos, *Phys. Rev. Lett.* **60**:1534 (1988).
5. G. P. Tsironis and St. Pnevmatikos, *Phys. Rev. B* **39**:7161 (1989).
6. A. Zolotaryuk and St. Pnevmatikos, *Phys. Lett. A* **143**:233 (1990).
7. P. S. Lomdahl and W. C. Kerr, *Phys. Rev. Lett.* **55**:1235 (1985).
8. K. Lindenberg and B. J. West, *The Nonequilibrium Statistical Mechanics of Open and Closed Systems* (VCH, New York, 1990).
9. E. S. Nylund and G. P. Tsironis, *Phys. Rev. Lett.* **66**:1886 (1991).
10. P. B. Hobbs, *Ice Physics* (Clarendon, Oxford, 1974).
11. H. Engelheart, B. Bullemer, and N. Riehl, *Physics of Ice*, N. Riehl, B. Bullemer, and H. Engelheart, eds. (Plenum Press, New York, 1969).
12. B. Klar, B. Hingerty, and W. Saenger, *Acta Cryst. B* **36**:1154 (1980); W. Saenger, Ch. Betzel, B. Hingerty, and G. M. Brown, *Nature* **296**:581 (1982).
13. H. Morgan and R. Pethig, *Int. J. Quantum Chem. Quantum Biol. Symp.* **11**:209 (1984).
14. W. Stoeckenius and W. H. Kunau, *J. Cell Biol.* **38**:337 (1968); D. Osterhelt and W. Stoeckenius, *Proc. Natl. Acad. Sci. USA* **70**:2853 (1973).
15. H. Merz and G. Zundel, *Biochem. Biophys. Res. Commun.* **156**:86 (1981).
16. P. C. Jordan, *J. Phys. Chem.* **91**:6582 (1987).
17. S. F. Fornili, D. P. Vercantern, and E. Clementi, *Biochem. Biophys. Acta* **771**:151 (1984); D. H. J. Mackay, P. H. Berens, K. R. Wilson, and A. T. Hagler, *Biophys. J.* **46**:229 (1984).
18. J. F. Nagle and S. Tristram-Nagle, *J. Membrane Biol.* **74**:1 (1983).
19. St. Pnevmatikos, A. V. Savin, and A. V. Zolotaryuk, in *Nonlinear Coherent Structures*, M. Barthes and J. Léon, eds. (Springer-Verlag, Berlin, 1990).